1   **The use of ASH-15 flowstone as a matrix-matched reference material for laser-ablation**

2   **U-Pb geochronology of calcite**

3   Perach Nuriel[1], Jörn-Frederik Wotzlaw[2], Maria Ovtcharova[3], Anton Vaks[1], Ciprian Stremtan[4],

4   Martin Šala[5], Nick M. W. Roberts[6], and Andrew R. C. Kylander-Clark[7]

6   [1] Geological Survey of Israel, 32 Yeshayahu Leibowitz St. Jerusalem, 9692100, Israel

7   [2] Institute of Geochemistry and Petrology, ETH Zurich, Clausiusstrasse 25 I CH-8092 Zurich,

8   Switzerland

9   [3] Department of Earth Sciences, University of Geneva, Geneva, Switzerland

10   [4] Teledyne Photon Machines, 384 Gallatin Park Drive, Bozeman, MT 59715, USA

11   [5] Department of Analytical Chemistry, National Institute of Chemistry, Hajdrihova 19, SI-1000

12   Ljubljana, Slovenia.

13   [6] Geochronology and Tracers Facility, British Geological Survey, Environmental Science

14   Centre, Nottingham, NG12 5GG, UK

15   [7] Department of Earth Science, University of California, Santa Barbara, CA 93106, USA.

17   **Abstract**

18   Latest advances in laser ablation inductively coupled plasma mass spectrometer (LA-ICPMS)

19   allow for accurate *in-situ* U-Pb dating of carbonate material, with final age uncertainties usually

20   >3% 2σ. Cross-laboratory reference materials (RMs) used for sample-bracketing are currently

21   limited to WC1 calcite with an age of 254.4 ± 6.5 (2σ). The minimum uncertainty on any age

22   determination with the LA-ICPMS method is therefore ≥ 2.5%, and validation by secondary

23   RMs is usually performed on in-house standards. This contribution present a new reference

24   material, ASH-15, a flowstone that is dated here by isotope dilution (ID) TIMS analysis using

25   37 sub-samples, 1-7 mg each. Age results presented here are slightly younger compared to

previous ID-IRMS U-Pb dates of ASH-15, but within uncertainties and in agreement with *in-situ* analyses using WC1 as the primary RM. We provide new correction parameters to be used as primary or secondary standardization. The suggested $^{238}U/^{206}Pb$ apparent age, not corrected for disequilibrium and without common-lead anchoring, is 2.965 ± 0.011 Ma (uncertainties are 95% confidence intervals). The new results could improve the propagated uncertainties on the final age with a minimal value of 0.4%, which is approaching the uncertainty of typical ID analysis on higher-U materials such as zircon. We show that although LA-ICPMS spot analyses of ASH-15 exhibit significant scatter in their isotopic ratios, the down-hole fractionation of ASH-15 is similar to that of other reference materials. This high-U (~1 ppm) and low Pb (<0.01 ppm) calcite is most appropriate as a reference material for other speleothem-type carbonates but requires more-sensitive ICP-MS instruments such as the new generation of single-collector and multi-collector ICP-MS. Reference materials with high Pb and low U or both low U and Pb compositions are still needed to fully cover the compositional range of carbonate material but may introduce analytical challenges.

Introduction

Recent advances in laser ablation techniques applied to multi-phase carbonates allow for accurate dating of a variety of sample types, including calcite cements (Li et al., 2014; Godeau et al., 2018; Anjiang et al., 2019; Holdsworth et al., 2019), hydrothermal veins (Coogan et al., 2016; MacDonald et al., 2019; Piccione et al., 2019), fault-related veins, breccia cement, and slickenfibers (Ring and Gerdes, 2016; Roberts and Walker, 2016; Goodfellow et al., 2017; Nuriel et al., 2017; Hansman et al., 2018; Parrish et al., 2018; Nuriel et al., 2019), and speleothems (Woodhead and Petrus, 2019). With increasing attention to climatic, seismic, and environmental events in the geological record, there is a growing need for dating techniques that can be accurate and easily implemented for samples at the sub-millimeter scale. This newly

50   emerging technique has the potential to contribute to our understanding of the duration, rate,

51   and extent of these important events in the geological record.

52   The *in-situ* approach has a great research potential for studying texturally complex samples

53   because it can resolve problems of age mixing of different phases or averaging of continuous

54   growth at the sub-millimeter scale, and thus increase the overall accuracy of the dated material.

55   While the precision of traditional isotope-dilution (ID) U-Pb analyses is still favorable (<1%

56   2σ) (Woodhead and Petrus, 2019), the increasing analytical development of the LA-ICPMS

57   method indicates the potential for improving the currently reported uncertainties (usually >3%

58   2σ). Finding the right matrix-matched reference material (RM) is a major hurdle for LA

59   analyses of carbonates because of the variety of mineralogy (calcite, dolomite, and aragonite),

60   textures, composition (e.g. high-magnesium calcite, high common-lead), and ages (e.g. low

61   radiogenic lead in young samples). Textural differences such as microcrystalline, fine- and

62   coarse-grained material, between the unknown and RMs can contribute to high uncertainties

63   due to differences in ablation efficiency, down-hole fractionation, and differences in crater

64   morphology (e.g. Guillong et al., 2020 and Elisha et al, 2020, this issue). Observed deviations

65   are potentially up to 20% of the final intercept age depending on the degree of crater geometry

66   mismatch and are related either to downhole fractionation and/or matrix effects (Guillong et

67   al., 2020).

68   Currently, the most commonly used procedure for mass-bias correction in the LA method, is

69   by standard-sample bracketing. For this, the $^{238}U/^{206}Pb$ LA-age of the RMs is corrected to the

70   true RM's $^{238}U/^{206}Pb$ apparent age (not corrected for disequilibrium) as measured

71   independently by an ID-IRMS method (ID-TIMS or ID-MC-ICPMS). The RMs are measured

72   throughout each session along with the unknown samples, and a normalization factor is applied

73   to correct both the RMs and the unknowns. Uncertainty propagation onto the age of the

74   unknowns includes the uncertainties of the 'true' RM age. As a result, the accuracy of the LA

75 analyses can only be as good as the uncertainties on the age of the RMs which is by itself

76 subjected to analytical challenges due to natural heterogeneities, impurities, and textural

77 complexities at the sub-millimetre scale. It is therefore essential that the 'true age' of the

78 reference material will reflect these complexities while maintaining minimal uncertainties.

79 Currently, several in-house standards are being used as reference materials, including Duff

80 Brown Tank (64 Ma; Hill et al., 2016), and JT (13.797 ± 0.031 Ma; Guillong et al., 2020). The

81 only well-characterized reference material that is distributed across laboratories is the WC1

82 calcite with an age of 254.4 ± 6.5 2σ (2.5%) (Roberts et al., 2017). The use of WC1 alone for

83 mass-bias correction has several disadvantages. First, it is highly recommended with all in situ

84 U-Th-Pb geochronology to use secondary RMs to validate any correction parameters that are

85 being used, and to appropriately propagate uncertainties. Second, the relatively high

86 uncertainty (2.5%) on the age of WC1 sets a minimal uncertainty on any LA U-Pb age

87 determination. Finally, the quantity of the WC1 sample that is currently available for future

88 work is limited and is likely to not fully meet the growing demands of the LA scientific

89 community; although we note here that there is a potential for further sample collection from

90 the original site.

91 **1** This contribution introduces a new carbonate reference material that can be widely used

92 for *in-situ* dating of calcite as primary or as cross-reference material with other available

93 standards. We characterise the reference material at various resolutions using a

94 combination of (1) laser ablation imaging (20 μm square beam); (2) LA spot analysis, ~80-

95 110 μm in diameter, conducted on both single-collector and multi-collector (MC)

96 inductively coupled plasma mass spectrometer (ICP-MS); and (3) ID-TIMS analyses of 37

97 sub-samples (~1-7 mg aliquots). We discuss several key issues related to the use of ASH-

98 15 sample as a RM, including down-hole fractionation, heterogeneities, and previous bulk

99   analyses, to provide the best correction parameters and suggested protocols for users of the

100   LA scientific community. **The ASH-15 flowstone**

101 The ASH-15 flowstone was found in Ashalim Cave, a karstic cave in the central Negev Desert

102 (30°56′36.2″ N, 34°44′22.5″ E), southern Israel, which is part of the northern margin of the

103 Saharan–Arabian desert belt. The cave entrance is located at an elevation of 414 m above sea

104 level and 67 km SE from the Mediterranean Sea coast. The cave is a three-dimensional

105 hypogene maze with a total length of 540 m, situated in Turonian limestone rock strata, at

106 depths of 0-31 m below the surface. The cave is richly decorated with vadose speleothems,

107 such as stalagmites, stalactites and flowstone, which are not active today because of the aridity

108 of the climate in the area (Vaks et al, 2010, 2018), but periods of their deposition correspond

109 to past episodes of wet climate in present-day desert. The thickness of the speleothems varies

110 from several cm to a few tens of cm. The soil above the cave is silicate loess, originated mainly

111 from aeolian dust (Crouvi et al., 2010) and the present day vegetation is composed of sparse

112 xeric shrubs with <10% vegetation cover.

113 The vadose speleothems of Ashalim Cave are composed of low-Mg calcite, and are divided

114 into a relatively thick Pliocene Basal layer, and thinner Pleistocene layers above it. The Basal

115 layer varies from 5 to 25 cm in thickness and comprises c. 90% of the speleothem volume in

116 the cave. It is composed of massive yellow calcite crystals (Fig. 1a-b), often showing

117 continuous growth in stalagmites and flowstone, suggesting deposition from continuously

118 dripping water. In all speleothems the Basal layer is terminated at its top by a <1 mm layer of

119 microcrystalline calcite, evaporite minerals and reddish clays (Fig. 1a), that is interpreted as a

120 hiatus (growth break) separating the Basal Pliocene layer and Quaternary layers above it (Vaks

121 et al., 2013). The thickness of Pleistocene top layers varies from several mm to 17 cm, but

122 usually does not exceed a few cm, comprising about 10% of the speleothem volume in the cave.

123 It is composed of alternating layers of brown calcite, with the youngest top layer (where found)

composed of yellow calcite. Several variably colored layers <1 mm thick of microcrystalline

calcite, evaporite minerals and reddish clays are found within the columnar crystalline structure,

suggesting hiatuses in speleothem deposition (Vaks et al., 2013).

The youngest periods of speleothem deposition in several Ashalim Cave speleothems were

dated by the ^{238}U-^{230}Th method and occurred from 221 ka to 190 ka and from 134 to 114 ka

(Vaks et al, 2010). Earlier periods of deposition were dated by the U-Pb method on ASH-15

flowstone at 1.272 ± 0.018 Ma (ASH-15-C), and the Basal layer of ASH-15 flowstone (layers

D-K) at c. ~3.1 Ma (Fig 1a). These layers have been dated in three different labs following

several protocols for ID analysis (Vaks et al., 2013; Mason et al., 2013). The U concentrations

in speleothem calcite range between 1.9 and 19.7 µg/g and the amounts of non-radiogenic Th

are negligible (Vaks et al., 2010).
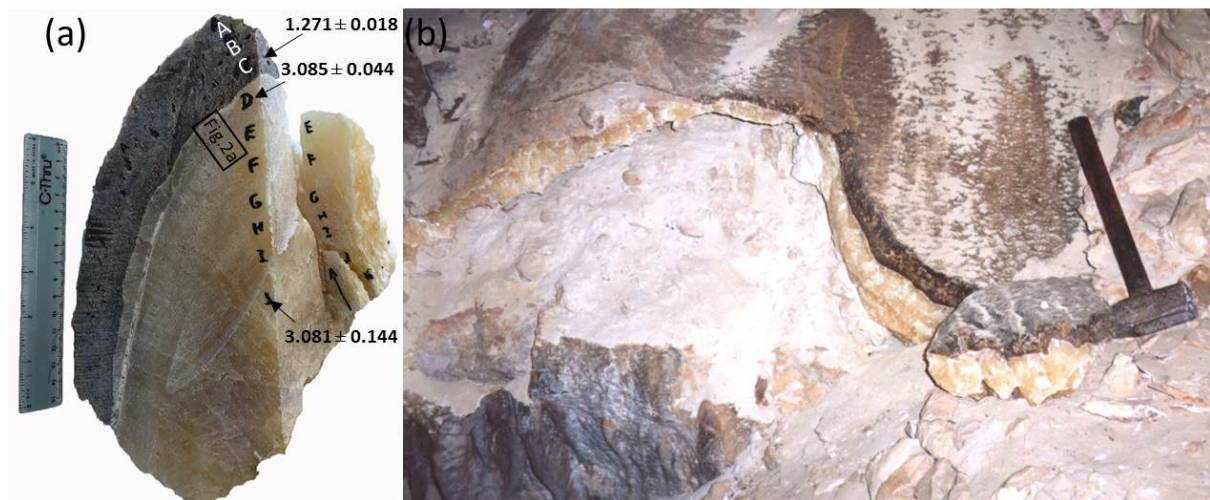
Figure 1. Sample ASH-15 from Ashalim Cave. (a) ~5 kg block of sample ASH-15 flowstone

consisting of the massive Pliocene yellow Basal layer (>2 cm calcite crystals; section D–K)

and the brown Quaternary layer (top section, A–C), the thin layer between the two stratigraphic

members represents a growth break (hiatus). The main U-Pb ages of Vaks et al., 2013 are

indicated; (b) In-situ flowstone within Ashalim Cave from which ASH-15 was sampled,

showing the large reservoir of this flowstone.

2 Sample ASH-15 textural characterization

The ASH-15 thin-section includes section D and E (see location in Fig.1a). Overall the thin-section examination indicates that the original texture is preserved with consistent growth direction, no observed hiatus, and no indications for dissolution and recrystallization. A spot analysis array, 85 μm in diameter, targeted along growth zone and along growth direction is visible in Fig. 2a-c. The ASH-15 sample shows no luminescence under cathodoluminescence light (Fig. 2c), suggesting formation under oxidising conditions. The slight bright luminescence observed within grain boundaries, discontinuities, and veins (arrows in Fig. 2b-c) may suggest the presence of fluid inclusions, textural differences, or some local replacement within these areas. These areas should be avoided if possible during spot analysis. The relatively homogenous low luminescence may suggest for a single-phase continuous calcite growth, whereby precipitation occurred relatively rapid from the same fluid source (e.g. with consistent Mn^{2+} Fe^{2+} composition) and/or under similar precipitation redox conditions. This 15 cm thick, ~3 Ma Pliocene layer (section D-K) is essentially of the same age. For this reason, previous dating of this sample also considered a similar initial $^{234}U/^{238}U$ activity ratio for disequilibrium correction (Mason et al., 2013; Vaks et al., 2013). The ASH-15 reference material consists of the whole Pliocene section that terminates with a sharp transition to the darker Pleistocene layers above it (section A-C; see Fig. 1b). About 3 kg of ASH-15 sample are excavated from the Ashalim Cave (Fig. 1a), and potentially much more can be sampled in the future (we estimate more than 10 kg of sample; Fig. 1b). The ASH-15 flowstone is therefore a good candidate for a reference material because of its large volume, high U concentrations, and potentially homogenous age which will be examine next.

165
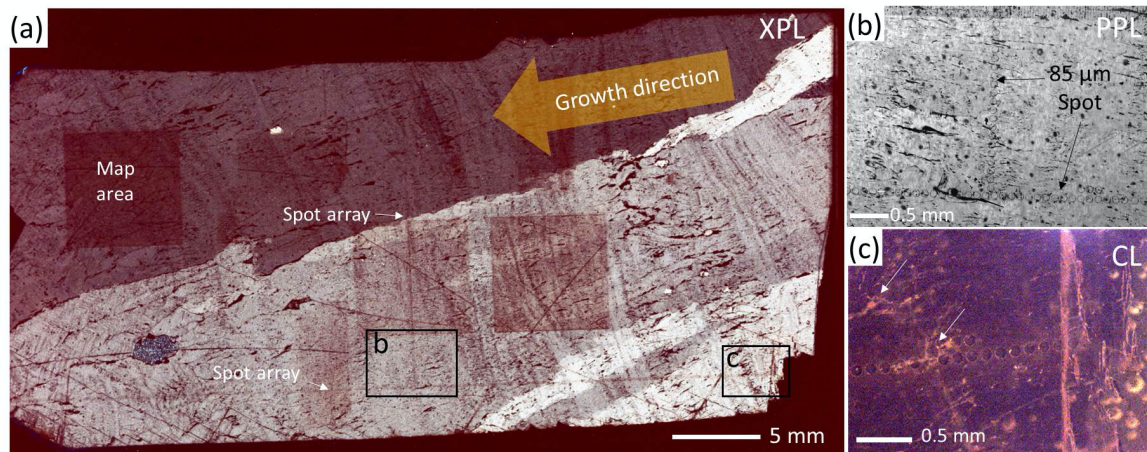
Figure 2. ASH-15D-E thin-section. (a) cross-polarized (XPL) scan , 36 mm long, showing

continuous growth (no hiatus), and consistent growth direction (indicated with yellow arrow).

Spot analyses are targeted either sub-parallel to growth zone or sub-parallel to growth direction;

(b) close-up on spot array analyses (location is shown in a) with 85 μm diameter; (c) CL image

showing no luminescence except for some bright luminescence within grains boundaries and

veins (arrows).

3   Methods

3.1   Elemental mapping

The sample ASH-15 was cut perpendicular to the growth zone of section D and E (see Fig.1b)

in order to examine heterogeneities across growth zone and within. Thin-sections were then

examined under plane- and cross-polarized light (XPL/PPL), and cathodoluminescence (CL)

microscopy (Fig. 2). The central part of the thin-section was also analyzed for elemental

distribution of selected elements. The elemental maps were measured via LA-ICPMS, carried

out on a 193 nm ArF excimer laser ablation system (Analyte G2 Teledyne Photon Machines

Inc., Bozeman MT) coupled to an ICP-QMS (Agilent 7900, Agilent Technologies, Santa Clara

CA). The laser was equipped with a Photon Machines HelEx II ablation chamber and an

Aerosol Rapid Introduction System (ARIS). The experiments were carried out using

acquisition parameters (both on the ICP and on the laser) modelled using the approach of van

184   Elteren et al (2019; 2018) to avoid artefacts (e.g., aliasing, smear, blur). All images (500x500

185   pixels) were acquired using a 20 μm square beam, fluence of 3.5 Jcm^{-2}, 294 Hz repetition rate

186   and dosage of 10 (10 overlapping pulses per spot size which amount to a scanning speed of

187   588 μms^{-1}). The masses monitored were ^{88}Sr, ^{137}Ba, ^{206}Pb, ^{208}Pb, ^{232}Th, and ^{238}U and the

188   images were constructed using Photon Machines' HDIP data reduction software (van Malderen,

189   2017).

3.2   LA-MC-ICPMS spot analyses

191   A thin section of ASH-15 was dated by U-Pb laser ablation multi-collector inductively coupled

192   plasma mass spectrometry (LA-MC-ICPMS) following the method described in Nuriel et al.

193   (2017). A Nu Plasma 3D was employed in conjunction with a Photon Machines Excite 193nm

194   Excimer laser equipped with a HelEex two volume cell. The laser was fired for 15 s during

195   analysis, using a repetition rate of 10 Hz, a spot size of 85 μm, and a fluence of approx. 1 J/cm^2.

196   The Nu Plasma 3D allows for the simultaneous acquisition of ^{238}U, ^{235}U, ^{232}Th, ^{208}Pb, ^{207}Pb,

197   ^{206}Pb, ^{204}Pb(+Hg), and ^{202}Hg, where ^{238}U-^{232}Th are measured on Faraday detectors and the low-

198   side masses are measured on Daly detectors. Instrumental mass-bias was corrected using a

199   two-step approach: both the ^{207}Pb/^{206}Pb and ^{206}Pb/^{238}U ratios were first corrected to NIST-614

200   glass reference material in *Iolite 3* using the geochronology reduction scheme (Paton et al.,

201   2010) to account for both mass-bias (^{207}Pb/^{206}Pb) and instrumental drift (^{207}Pb/^{206}Pb and

202   ^{206}Pb/^{238}U). The Tera-Wasserburg data, output from *Iolite*, was then plotted and ^{206}Pb/^{238}U

203   ratios of all RMs and unknowns were adjusted such that the primary calcite reference

204   material—WC-1—yielded an age of 254 Ma (Roberts et al., 2017). This resulted in accurate

205   dates for both our secondary calcite RM: Duff Brown Tank at 66.8 ± 3.4 Ma (previously

206   reported 64 Ma; Hill et al., 2016) and a ^{207}Pb/^{206}Pb date of zircon RM at 566.0 ± 2.8 Ma

207   (previously reported 564 Ma; Gehrels et al., 2008). Uncertainty propagation of individual ratios

208   was assessed by reproducibility of the NIST614 and SL RMs (n=44 in both cases) and added

209 in quadrature such that the MSWD of each weighted average is ≤1 and that the uncertainty is

210 no better than 2% (long-term reproducibility); this resulted in propagated uncertainties of 2.5%

211 and 2% for the $^{206}Pb/^{238}U$ and $^{207}Pb/^{206}Pb$ ratios, respectively. Given that the typical

212 uncertainties of the $^{206}Pb/^{238}U$ and $^{207}Pb/^{206}Pb$ ratios of the unknowns was >10% and >3%,

213 respectively, the uncertainty propagation on individual ratios had little effect on the calculation

214 of the final date of ASH-15. The thin section of ASH-15 was measured both parallel to the

215 length of section (303 spots, and perpendicular to it (101 spots). Data are plotted using Isoplot

216 (Ludwig, 1998).

217

218 **3.3   LA-ICPMS spot analyses**

219 Analyses were conducted at the Geochronology and Tracers Facility, British Geological

220 Survey (Nottingham, UK). The instrumentation comprised a New Wave Research 193UC

221 excimer laser ablation system fitted with a TV2 cell, coupled to a Nu Instruments Attom single

222 collector ICP-MS. The method follows the protocols described in Roberts and Walker (2016)

223 and Roberts et al. (2017). Laser parameters varied slightly per session, but typically involve a

224 pre-ablation cleaning spot of 150 µm, fired at 10 Hz with a fluence of ~6 J/cm^2 for 2 seconds,

225 and ablation conditions of 80-100 µm spots, fired at 10 Hz with a fluence of ~6-8 J/cm^2 for 25-

226 30 seconds. A 60 second background is taken before every set of standard-bracketed analyses,

227 and a 5 second washout is left between each ablation. Normalization of Pb-Pb ratios is achieved

228 using NIST614 glass (values of Woodhead and Hergt, 2001), and WC-1 carbonate for Pb-U

229 ratios (Roberts et al., 2017). Data reduction uses the Time Resolved Analysis function of the

230 Nu Instruments Attolab software, and an excel spreadsheet, with uncertainty propagation

231 following the recommendations of Horstwood et al. (2016).

232

3.4 ID-TIMS U-Pb geochronology

Isotope dilution thermal ionization mass spectrometry (ID-TIMS) U-Pb geochronology was performed at the Institute of Geochemistry and Petrology of ETH Zurich (ETHZ) and at the Department of Earth Sciences of the University of Geneva (UNIGE). Millimetre-sized chips of the ASH-15-D and ASH-15-K calcite were extracted using stainless steel tools. Larger chips were further sub-divided resulting in ~1-7 mg aliquots. Individual chips were transferred into 3 ml Savillex beakers and repeatedly ultrasonically cleaned in ultrapure acetone and water. Cleaned sampled were transferred into pre-cleaned 3 ml Savillex beakers, spiked with ~5-10 mg EARTHTIME (^{202}Pb-)^{205}Pb-^{233}U-^{235}U tracer solution (Condon et al., 2015) and dissolved in 6N HCl at 120°C on a hotplate for ~30 minutes to assure complete dissolution and sample-spike equilibration. Dissolved samples were dried down and redissolved in 1N HBr. Uranium and Pb were separated using a single-column (50 µl, AG1-X8 resin) HBr-HCl anion exchange chemistry. The Pb fraction was dried down with a drop of H_3PO_4 after a single column pass. Uranium was dried down, redissolved in 3N HCl and further purified with a HCl-based second column pass before drying it down with a drop of H_3PO_4. Uranium and Pb were loaded on outgassed single Re filaments with ~1 µl of Si-gel emitter for thermal ionization mass spectrometry. Uranium and Pb isotope ratios were measured on a Thermo TRITON Plus at ETHZ and a Thermo TRITON at UNIGE. Lead isotopes were measured on the axial secondary electron multiplier employing dynamic peak-hopping routine collecting masses (202), 204, 205, 206, 207 and 208. Measured Pb isotope ratios were corrected for mass fractionation either using the double spike (ETHZ) or using a mass fractionation factor of 0.15 ± 0.03 %/amu for single Pb spiked samples (UNIGE). Uranium isotope ratios were measured as uranium-oxide (UO_2) employing a static measurement routine with Faraday cups connected to amplifiers with 10^{13} ohm feedback resistors (von Quadt et al., 2016; Wotzlaw et al., 2017). Isotope ratios were corrected for isobaric interferences from minor UO_2 isotopologues (Wotzlaw et al., 2017) and

258 for mass fractionation using the double spike assuming a $^{238}U/^{235}U$ ratio of 137.818 ± 0.045

259 (Hiess et al., 2012) for sample and blank. Total procedural Pb blanks for the HBr-based

260 chemistry at ETHZ are consistently between 0.2 and 0.4 pg. We therefore attribute up to 0.4

261 pg to laboratory blank with the remaining common Pb being attributed to initial common Pb.

262 Total procedural blanks measured at UNIGE yielded an average of 1.15 pg that was taken as

263 the laboratory blank contribution. Data reduction and uncertainty propagation was performed

264 using Tripoli and an Microsoft Excel-based spreadsheet that uses the algorithms of Schmitz

265 and Schoene (2007). Isochron calculations were performed using IsoplotR (Vermeesch, 2018).

266 All uncertainties are reported at 95% confidence ignoring systematic uncertainties associated

267 with the tracer calibration and decay constants unless otherwise stated.

268 **4 Results**

269 All analyses were performed on ASH-15-D-K yellow Pliocene layer, abbreviated here as

270 "ASH-15" unless specification of ASH-15-D, E etc. is indicated. The ASH-15-A-C brown

271 Pleistocene layer is not part of the ASH-15 suggested reference material.

272 **4.1 LA elemental mapping**

273 Elemental mapping for ^{88}Sr, ^{137}Ba, ^{206}Pb, ^{208}Pb, ^{238}U and $^{238}U/^{206}Pb$ ratio shows that the

274 distribution of most elements is relatively homogeneous (Fig.3), and in good accordance with

275 the luminescence data. Higher intensities for ^{238}U and ^{88}Sr were observed along grain

276 boundaries and discontinuities, whereas Pb and the rest of the trace elements are more

277 homogeneously distributed, arguing for steady environmental conditions during the deposition.

278 Ten random regions of interest (ROI) were selected throughout the sample to mimic 10 spot

279 analysis carried out at 85-90 microns spot size – just like one would do for U-Pb geochronology.

280 These ROIs were generated by drawing on the map circular regions with the radius of 85 or 90

281 microns in diameter. The pixels comprising each ROI were pooled together as representing the

282 equivalent of a single spot analysis. The statistical data for each cluster (data are given in

283 supplementary file) were compared. The average values for all pixel data are within 2 standard

284 errors and in good agreement, indicating that, at least based on the elemental distribution we

285 measured, the sample is relatively homogeneous for a natural sample. To further investigate

286 the chemical homogeneity of the sample, a random transect through one of the growth zones

287 was drawn and the signal intensities for ^{238}U were extracted. The transect data also indicate

288 that ^{238}U variations are within 2 standard errors of the average value (full data is available in

289 Table S1 in the supplement).
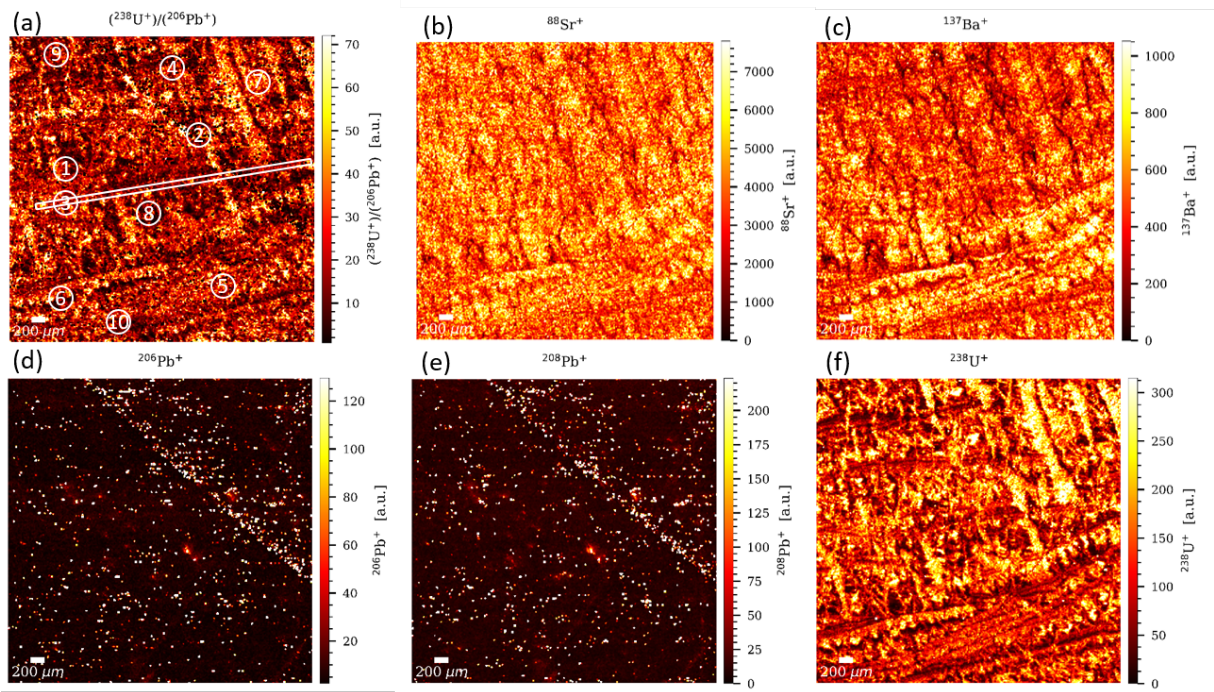
290

291 **Figure 3.** Signal intensity maps of ASH-15. For ^{238}U/^{206}Pb, ^{88}Sr, ^{137}Ba, ^{206}Pb, ^{208}Pb, and ^{238}U

292 (a-d). The plotted signal was corrected for blank and analytical drift of the instrumentation.

293 Note that each distribution map has its own signal intensity scale. The position of the regions

294 of interest and transect is shown in (a). The circles designating the location of the regions of

295 interest are not at scale (data is available in Table S1 in the supplement).

296 **4.2 LA-MC-ICPMS spot analyses**

297 Data and calculated ages for the LA-MC-ICPMS transects are shown in Tera-Wasserburg

298 space in Fig. 4 (n = 379 of 412 total spots). Analyses rejected from the age calculation include

299 those with $^{207}Pb/^{206}Pb$ uncertainties larger than 0.1% (n = 2) and those with high common-Pb

300 contents (^{208}Pb cps >5000; n = 17). A further 14 spots plotted below the array; these data

301 represent the first 1–2 mm of spots of the lengthwise transect (lower right in Fig. 2a), and

302 suggest that a small percent of ASH-15 may behave differently during ablation and/or may

303 have been subsequently modified after crystallization; upon inspection, this portion of the

304 section contains more pore space and impurities than the majority of the section. The remaining

305 379 define a normally distributed array with a lower intercept age of 2.952 ± 0.043 Ma (MSWD

306 = 2.5), which is well within uncertainty of the new ID-TIMS data presented (full data is

307 available in Table S2 in the supplement). The calculated upper intercept of each transect is

308 equivalent and within 1% of the common Pb composition calculated from the ID-TIMS data.

309 Not surprisingly, the lengthwise transect reveals a larger spread in common/radiogenic Pb

310 ratios; this transect crosses more growth zones and has a higher probability of sampling a

311 variety of concentrations of both Pb and U. Conversely, the more limited spread in

312 common/radiogenic Pb ratios appears to reflect the limited sampling of growth zones, and

313 would suggest that individual growth zones contain a relatively limited range of concentrations

314 in U and Pb. The slightly higher MSWD for the lengthwise transect (2.7) relative to the growth

315 zone transect (2.5) could also reflect these inherited compositional differences during growth

316 history, and a resulted "mixing" or "averaging" of different growth phase along calcite

317 continuous growth.

318 Variations of ASH-15 ages during 20 different runs (with 5-30 spot analysis in each) using

319 both single-collector and multi-collector ICP-MS are shown in Fig. 4b (full data is available in

320 Tables S3-S5 in the supplement). The ages are calculated using IsoplotR, not anchored to

321 specific common-lead, and are not corrected for disequilibrium. Although there is a large

322   scatter in the ages of the different runs the average ages (marked with black box) plot close to

323   the new ID-TIMS ages, or are slightly younger in age.
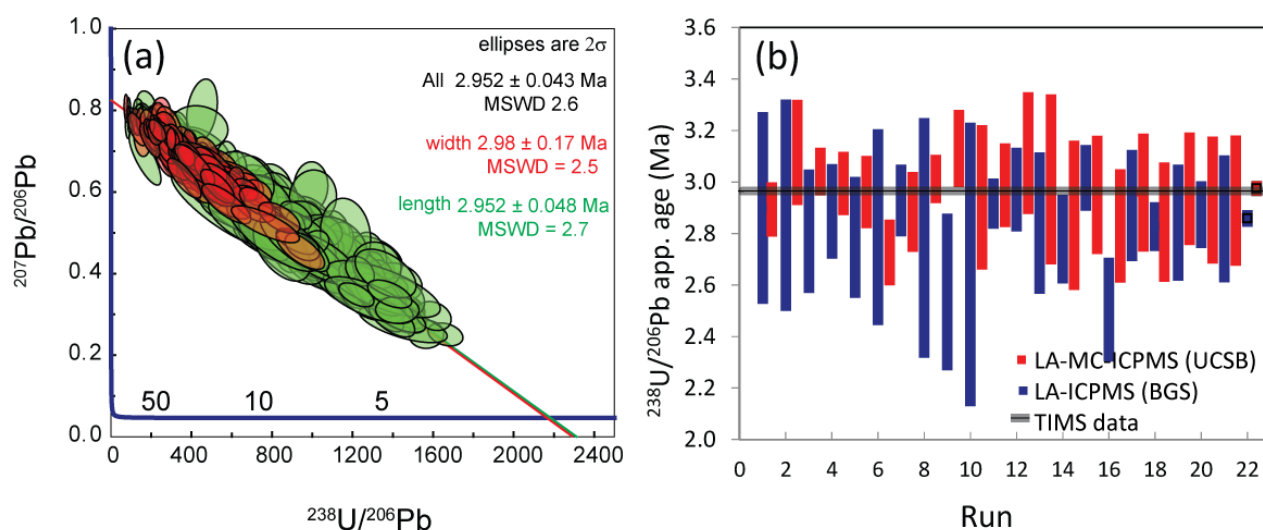
324

325   **Figure 4.** LA-MC-ICPMS analyses of calcite ASH-15. (a) Tera-Wasserburg concordia space

326   plot (n=385) for spots analysis within lengthwise transect (green) and along growth zone

327   transect (red). Calculated age, 2σ error and MSWD are given for both and for all spots together;

328   (full data is available in Table S2 in the supplement); (b) Variations of ASH-15 ages during

329   different runs using both single-collector (at the British Geological Survey) and multi-collector

330   (at University of California Santa Barbara) ICP-MS. Ages are calculated using WC1 as primary

331   RM; the new ID-TIMS age is indicated with a grey line; (full data is available in Table S3-S5

332   in the supplement).

333   **4.3   Down-hole fractionation**

334   Reference material is important for correction of both laser-induced elemental fractionation

335   (LIEF) and plasma-related ionization efficiency.   Ideally, the reference material should

336   resemble the unknown samples as much as possible in terms of its chemistry (e.g. Mg and Fe

337   content), texture (i.e. micritic, crystalline), and age. The WC1 and ASH15 are both low-Mg

338   calcite but they are very different in textures and age. The ASH15 is a ~3 Ma, well-crystallized

339   elongated calcite (up to 1 cm) and WC1 is a 254 Ma recrystallized botryoidal calcite, formed

340   after aragonite. Despite these differences, both WC1 and ASH15 display a very similar down-

341   hole fractionation pattern (Fig. 5d). Fig. 5 shows stacked integration plots of the down-hole

342   raw ^{206}Pb/ ^{238}U ratio of different RMs including, the ASH15, WC-1, and Duff Brown Tank

343   (Black and Gulson, 1978). The ASH15 displays much larger scatter in the raw data (Fig. 5a) in

344   comparison to both WC1 and Duff Brown Tank (Fig. 5b-c), however, the average value yielded

345   identical down-hole fractionation to that of WC-1 (Fig. 5d). Duff Brown Tank is also consistent

346   with the down-hole patterns but less steep in comparison to WC1 and ASH15 (Fig. 5d). This

347   comparison suggests that down-hole fractionation and laser-induced elemental fractionation

348   (LIEF) are similar among the different RMs. It is thus suggested that differences in measured

349   and expected ^{206}Pb/^{238}U ratios in calcite material are likely to be caused mostly by plasma-

350   ionization differences between unknown samples and RMs.

351
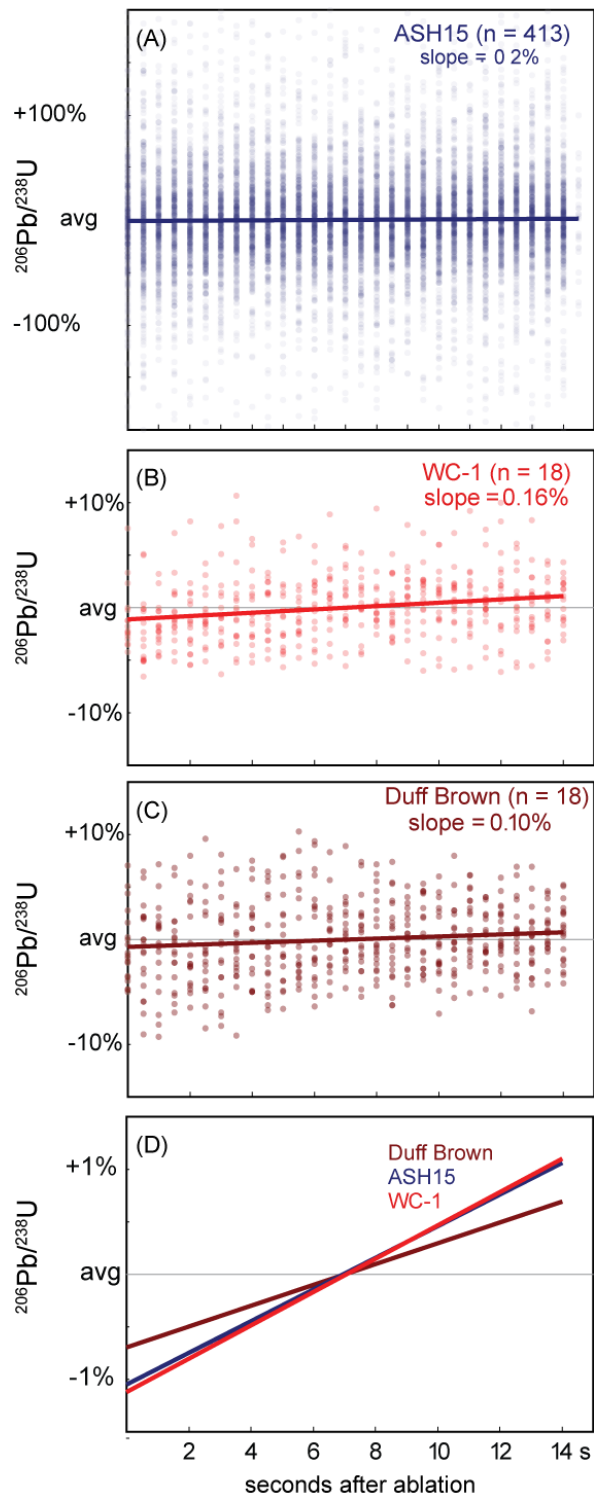
Figure 5. Stacked integration plots of raw [207]Pb-corrected [206]Pb/[238]U ratios for calcite reference

materials ASH-15, WC-1, and Duff Brown Tank. The low Pb concentration in ASH-15 yields

more scatter, but average slopes of all RMs are similar, with 1-2% change in age over 10

seconds (100 pulses) of ablation. The results suggest minimal differences in down-hole

fractionation of the different RMs.

4.4   ID-TIMS results

Twelve aliquots of ASH-15D analyzed at ETHZ yielded ^{238}U/^{206}Pb ratios between 1096 and 2084 and ^{207}Pb/^{206}Pb ratios between 0.0825 and 0.4403 (full data is available in Table S6 in the supplement). Plotted in Tera-Wasserburg space, these data yield a single isochron with an initial ^{207}Pb/^{206}Pb of 0.832 ± 0.015 (uncertainties are 95% confidence intervals) and a concordia intercept age of 2.967 ± 0.022 Ma (Fig. 6a). The elevated mean square weighted deviation (MSWD) of 12 is attributed to minor heterogeneities, most likely in the initial ^{207}Pb/^{206}Pb ratio of the speleothem calcite. Twelve aliquots of ASH-15K analyzed at ETHZ returned ^{238}U/^{206}Pb ratios between 723 and 2094 and ^{207}Pb/^{206}Pb ratios between 0.0720 and 0.5677. In Tera-Wasserburg space, eleven out of twelve aliquots define a isochron with an initial ^{207}Pb/^{206}Pb of 0.8314 ± 0.0040 and a concordia intercept age of 2.964 ± 0.016 Ma (Fig. 6b). A single aliquot (#5.4) plots significantly below the isochron defined by the other aliquots. The elevated MSWD of 34 together with the single outlier suggest some heterogeneities in the initial ^{207}Pb/^{206}Pb of the ASH-15K calcite. Thirteen aliquots of ASH-15K analyzed at UNIGE (pink color, Fig. 6b) yielded ^{238}U/^{206}Pb ratios between 433 and 1853 and and ^{207}Pb/^{206}Pb ratios ranging from 0.1856 to 0.6660. Twelve of the thirteen analyses yield best-fit line with an initial ^{207}Pb/^{206}Pb of 0.814 ± 0.019 and a Concordia intercept age of 2.947 ± 0.065 Ma. The elevated MSWD of 36 confirms the minor heterogeneity of the initial ^{207}Pb/^{206}Pb.

The excellent agreement between the ASH-15D and ASH-15K datasets indicates that the entire speleothem growth layer between these two growth zones is of equivalent age with minor heterogeneities in the initial ^{207}Pb/^{206}Pb ratio and justifies combining the data into a single isochron regression. The combined isochron, using 35 of 37 analyzed aliquots, yields an initial ^{207}Pb/^{206}Pb of 0.8306 ± 0.0033 and a concordia intercept age of 2.965 ± 0.011 Ma with a MSWD of 35 (Fig. 6c). We consider the results of the combined regression as the best reference value for using ASH-15 as a primary reference material.

The new TIMS data provide the most extended bulk investigation of the ASH-15 sample, with a total of 37 sub-samples that are separated from bottom (K, n=25) to top (D, n=12). The high MSWD of 35 is suggested to reflect true heterogeneities of the dated material, possibly related to impurities that are concentrated within grain boundaries (as suggested by CL and elemental mapping). We re-calculated previously determined isochron ages of Vaks et al. (2013) and Mason et al. (2013; Fig. 7). We obtained concordia intercept ages of 3.0088 ± 0.053 Ma for ASH-15-D (MSWD=11; n=5) and 3.0153 ± 0.042 Ma for ASH-15-K (MSWD=14; n=5) of Vaks et al. (2013) and 3.0015 ± 0.029 for ASH-15-D (MSWD=2; n=5) of Mason et al. (2013). These ages are largely overlapping within uncertainty with our new ID-TIMS age of 2.965 ± 0.011 Ma (Fig. 7; and data in Table S7 in the supplements). The apparent minor systematic offset towards slightly older ages is attributed to the lower number of aliquots in the MC-ICPMS datasets combined with the heterogeneous initial Pb isotope composition. For laser ablation U-Pb work, we recommend the use of the new ID-TIMS age because of the large number of sub-samples (n=37), and the small aliquots (1-7 mg) that are more representative of laser-ablation spot analysis. In addition, the use of the precisely and accurately calibrated EARTHTIME tracer solutions (Condon et al., 2015) and the online mass fractionation correction provided by the double Pb and double U tracer are an important advantage of this method. The excellent interlaboratory reproducibility gives us additional confidences that our ID-TIMS data provide the most accurate characterization of the U-Pb systematics of the ASH-15 calcite for use as a primary reference material.

402
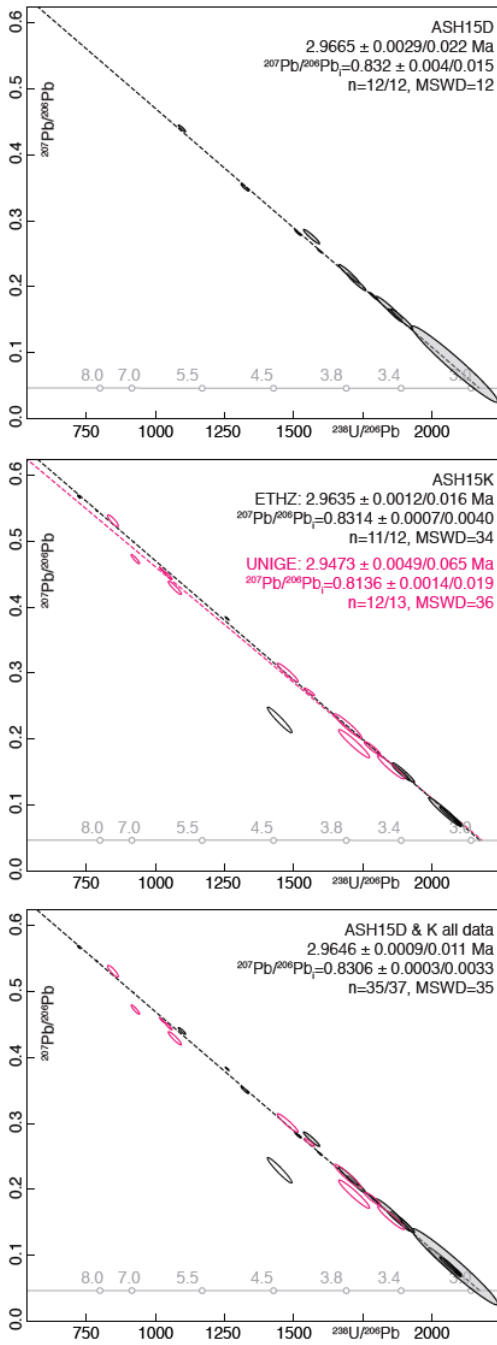
Figure 6. ID-TIMS U-Pb results for ASH-15D, ASH-15K, and for both ASH-15D+K displayed in Tera-Wasserburg concordia space. Uncertainties on the initial [207]Pb/[206]Pb ratios and the intercept ages are reported at 95% confidence including overdispersion (Vermeesch, 2018).
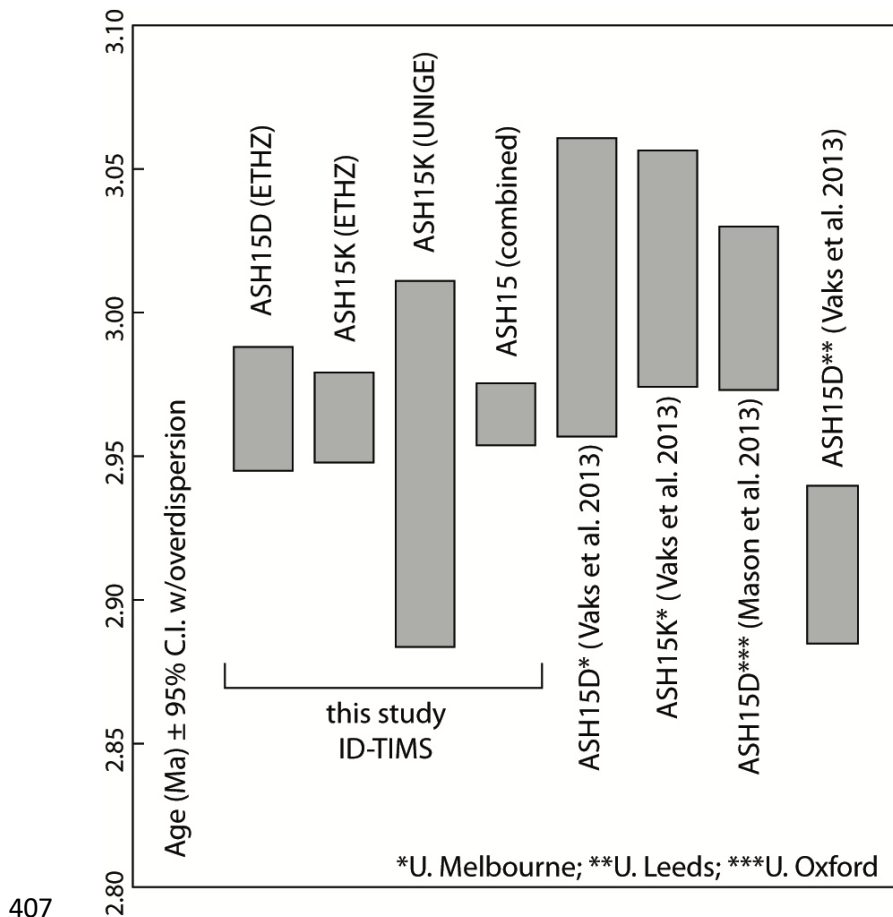
Figure 7. Previous (re-calculated) and new ages of ASH-15 from isotope-dilution U-Pb analysis. All ages are calculated using IsoplotR (Vermeesch, 2018), are not corrected for disequilibrium and are not anchored to common-lead specific value (see data in Table S7 in the supplements).

4.5 Calcite reference material

The U and Pb concentrations of carbonate materials vary greatly. Data compilation by Roberts et al. (2020; this issue) combined hundreds of carbonate samples from different origin such as diagenetic, biogenic, speleothem, and vein-fill. This compilation indicates several orders of magnitude differences in U and Pb concentrations of the different types of carbonate and the heterogeneity of spot analysis within each type or even a single sample. A modified representation of their data, excluding calcite vein-fill, which vary throughout the entire

419   compositional range, is shown together with the currently available calcite reference materials

420   (Fig. 8; and full data in Table S8 in the supplement). Note that both ASH15 and JT, display

421   much larger heterogeneity when measured by LA-ICPMS (small symbols) relative to ID-TIMS

422   (large symbols). Despite the high compositional heterogeneity of each of the reference material,

423   they show minimal overlap and together they cover most of the compositional range of the

424   presented carbonate material. WC1 (Roberts et al., 2017) with relatively high U and Pb

425   concentrations can easily be measured on less-sensitive ICP-MS such as quadrupole

426   instruments, and is most appropriate to be used for dating vein-fill and diagenetic carbonates.

427   In contrast, the ASH15 flowstone, with relatively low Pb and high U concentration that are

428   better measured on more-sensitive ICP-MS (e.g. new generation of single-collector and multi-

429   collector ICP-MS), and is most appropriate for dating speleothem type carbonates. Finally the

430   JT (Guillong et al., 2020), with moderate U and Pb concentration can be used can be used for

431   most single- collector and multi-collector sector-field ICP-MS instrument as well as the newer

432   generation of quadrupole ICP-MS. Reference material with high Pb and low U or both low U

433   and Pb concentrations will further help to cover the full compositional range of carbonate

434   material but may introduce analytical challenges.

435
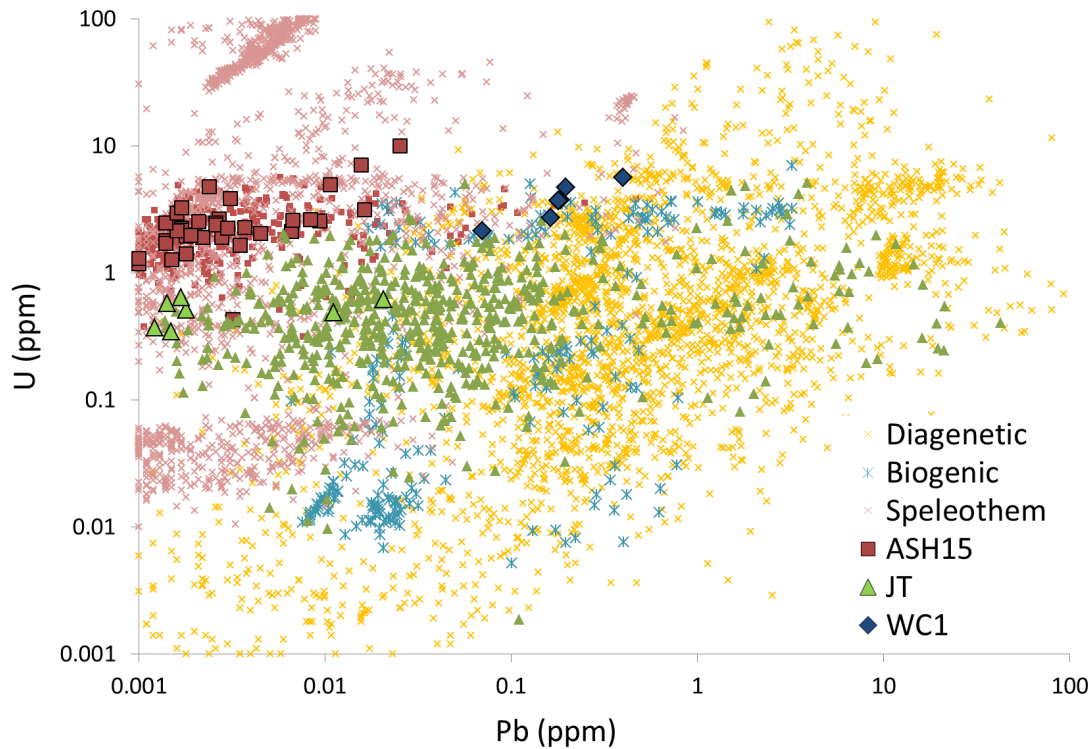
Figure 8. U and Pb concentrations of different carbonate samples and available reference materials. Large and small symbols for the reference materials indicate ID-TIMS and LA-ICPMS analyses, respectively. Note the minimal compositional overlap of the three reference materials (ASH15, WC1, and JT). Data for diagenetic, biogenic, and speleothem carbonates are from Roberts et al. (2020, this issue). Data for JT standard are from Guillong et al. (2020).

5 Conclusions

The ASH-15 speleothem calcite is characterized as a matrix matched reference material for LA-ICPMS U-Pb geochronology of calcite. ID-TIMS analyses of small 1-7 mg aliquots of two growth zones suggest sufficient homogeneity with a combined intercept age of 2.965 ± 0.011 Ma and an initial $^{207}Pb/^{206}Pb$ of 0.8315 ± 0.0026. These data are recommended as the reference values for the ASH-15 calcite reference material. The excellent agreement between the two growth zones suggest that the entire interval between the two dated layers can be used with the same reference age. Compared to other calcite reference material (e.g. WC1), ASH-15 is more

homogeneous but has lower radiogenic Pb content and therefore requires more sensitive instruments (i.e. sector field rather than quadrupole mass spectrometers) to be used as a reference material.

Author's contribution

PN: data processing and writing, JFW: ID-TIMS analysis and writing, MO: ID-TIMS analysis, AV: sample collection and writing, CS: LA mapping analysis and writing, MS: LA mapping analysis. NR: LA-ICPMS, data analysis and writing. AKC: LA-MC-ICPMS, data analysis and writing.

Competing interests

The authors declare that they have no conflict of interest.

Acknowledgements

We thank reviewers Fernando Corfu and Jon Woodhead as well as editor Axel Gerdes for constructive comments and suggestions. We thank Bar Elisha for thin-section preparation and Andrew Mason for constructive discussion. This study was funded by the Israel Science Foundation, Grant ISF-727/16.

469   **Appendices**
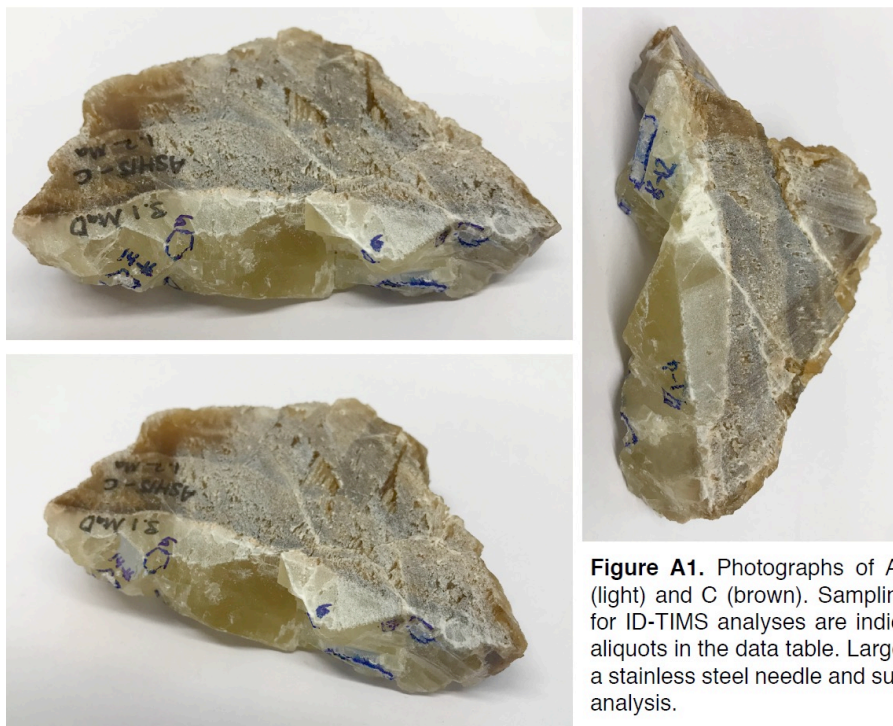
Figure A1. Photographs of ASH15 flowstone with layers D (light) and C (brown). Sampling localities of aliquots sampled for ID-TIMS analyses are indicated by numbers matching the aliquots in the data table. Larger pieces were chipped off using a stainless steel needle and subdivided into smaller aliquots for analysis.

470

Figure A2. Photographs of ASH15 flowstone with layers K (bottom) to D (top). Sampling localities of aliquots samples for ID-TIMS analyses within layer K are indicated with numbers (n=12) and are matching the aliquots in the data table.

471

References:

Anjiang, S., Anping, H., Cheng, T., Liang, F., Wenqing, P., Yuexing, F., and Zhao, J.: Laser ablation in situ U-Pb dating and its application to diagenesis-porosity evolution of carbonate reservoirs, 46, 1127-1140, 2019.

Condon, D., Schoene, B., McLean, N., Bowring, S., and Parrish, R.: Metrology and traceability of U–Pb isotope dilution geochronology (EARTHTIME Tracer Calibration Part I), Geochimica et Cosmochimica Acta, 164, 464-480, 2015.

Coogan, L. A., Parrish, R. R., and Roberts, N. M.: Early hydrothermal carbon uptake by the upper oceanic crust: Insight from in situ U-Pb dating, Geology, 44, 147-150, 2016.

Crouvi, O., Amit, R., Enzel, Y., and Gillespie, A. R.: Active sand seas and the formation of desert loess, Quaternary Science Reviews, 29, 2087-2098, 2010.

Godeau, N., Deschamps, P., Guihou, A., Leonide, P., Tendil, A., Gerdes, A., Hamelin, B., and Girard, J.-P. J. G.: U-Pb dating of calcite cement and diagenetic history in microporous carbonate reservoirs: Case of the Urgonian Limestone, France, 46, 247-250, 2018.

Goodfellow, B. W., Viola, G., Bingen, B., Nuriel, P., and Kylander-Clark, A. R. C.: Palaeocene faulting in SE Sweden from U–Pb dating of slickenfibre calcite, Terra Nova, n/a-n/a, 10.1111/ter.12280, 2017.

Guillong, M., Wotzlaw, J. F., Looser, N., and Laurent, O.: New analytical and data evaluation protocols to improve the reliability of U-Pb LA-ICP-MS carbonate dating, Geochronology Discuss., 2020, 1-17, 10.5194/gchron-2019-20, 2020.

Hansman, R. J., Albert, R., Gerdes, A., and Ring, U.: Absolute ages of multiple generations of brittle structures by U-Pb dating of calcite, Geology, 46, 207-210, 2018.

Hiess, J., Condon, D. J., McLean, N., and Noble, S. R.: 238U/235U systematics in terrestrial uranium-bearing minerals, Science, 335, 1610-1614, 2012.

Holdsworth, R., McCaffrey, K., Dempsey, E., Roberts, N., Hardman, K., Morton, A., Feely, M., Hunt, J., Conway, A., and Robertson, A.: Natural fracture propping and earthquake-induced oil migration in fractured basement reservoirs, Geology, 47, 700-704, 2019.

Horstwood, M. S., Košler, J., Gehrels, G., Jackson, S. E., McLean, N. M., Paton, C., Pearson, N. J., Sircombe, K., Sylvester, P., and Vermeesch, P.: Community-derived standards for LA-ICP-MS U-(Th-)Pb geochronology–Uncertainty propagation, age interpretation and data reporting, Geostandards and Geoanalytical Research, 40, 311-332, 2016.

Li, Q., Parrish, R., Horstwood, M., and McArthur, J.: U–Pb dating of cements in Mesozoic ammonites, Chemical Geology, 376, 76-83, 2014.

MacDonald, J., Faithfull, J., Roberts, N., Davies, A., Holdsworth, C., Newton, M., Williamson, S., Boyce, A., John, C. J. C. t. M., and Petrology: Clumped-isotope palaeothermometry and LA-ICP-MS U–Pb dating of lava-pile hydrothermal calcite veins, 174, 63, 2019.

Mason, A. J., Henderson, G. M., and Vaks, A.: An Acetic Acid-Based Extraction Protocol for the Recovery of U, Th and Pb from Calcium Carbonates for U-(Th)-Pb Geochronology, Geostandards and Geoanalytical Research, 37, 261-275, 10.1111/j.1751-908X.2013.00219.x, 2013.

Nuriel, P., Weinberger, R., Kylander-Clark, A. R. C., Hacker, B. R., and Craddock, J. P.: The onset of the Dead Sea transform based on calcite age-strain analyses, Geology, *45*, 587-590, 10.1130/g38903.1, 2017.

Nuriel, P., Craddock, J., Kylander-Clark, A. R., Uysal, I. T., Karabacak, V., Dirik, R. K., Hacker, B. R., and Weinberger, R. J. G.: Reactivation history of the North Anatolian fault zone based on calcite age-strain analyses, 47, 465-469, 2019.

Parrish, R. R., Parrish, C. M., and Lasalle, S.: Vein calcite dating reveals Pyrenean orogen as cause of Paleogene deformation in southern England, Journal of the Geological Society, 10.1144/jgs2017-107, 2018.

Piccione, G., Rasbury, E. T., Elliott, B. A., Kyle, J. R., Jaret, S. J., Acerbo, A. S., Lanzirotti, A., Northrup, P., Wooton, K., and Parrish, R. R.: Vein fluorite U-Pb dating demonstrates post–6.2 Ma rare-earth element mobilization associated with Rio Grande rifting, Geosphere, 15, 1958-1972, 2019.

Ring, U., and Gerdes, A.: Kinematics of the Alpenrhein-Bodensee graben system in the Central Alps: Oligocene/Miocene transtension due to formation of the Western Alps arc, Tectonics, 35, 1367-1391, 10.1002/2015TC004085/abstract, 2016.

Roberts, N. M., and Walker, R. J.: U-Pb geochronology of calcite-mineralized faults: Absolute timing of rift-related fault events on the northeast Atlantic margin, Geology, 44, 531-534, 2016.

Roberts, N. M., Rasbury, E. T., Parrish, R. R., Smith, C. J., Horstwood, M. S., and Condon, D. J.: A calcite reference material for LA-ICP-MS U-Pb geochronology, Geochemistry, Geophysics, Geosystems, 2017.

Roberts, N. M. W., Drost, K., Horstwood, M. S. A., Condon, D. J., Chew, D., Drake, H., Milodowski, A. E., McLean, N. M., Smye, A. J., Walker, R. J., Haslam, R., Hodson, K., Imber, J., Beaudoin, N., and Lee, J. K.: Laser ablation inductively coupled plasma mass spectrometry (LA-ICP-MS) U–Pb carbonate geochronology: strategies, progress, and limitations, Geochronology, 2, 33-61, 10.5194/gchron-2-33-2020, 2020.

Schmitz, M. D., and Schoene, B.: Derivation of isotope ratios, errors, and error correlations for U-Pb geochronology using 205Pb-235U-(233U)-spiked isotope dilution thermal ionization mass spectrometric data, Geochemistry, Geophysics, Geosystems, 8, 2007.

Vaks, A., Bar-Matthews, M., Matthews, A., Ayalon, A., and Frumkin, A.: Middle-Late Quaternary paleoclimate of northern margins of the Saharan-Arabian Desert: reconstruction from speleothems of Negev Desert, Israel, Quaternary Science Reviews, 29, 2647-2662, 2010.

Vaks, A., Woodhead, J., Bar-Matthews, M., Ayalon, A., Cliff, R. A., Zilberman, T., Matthews, A., and Frumkin, A.: Pliocene–Pleistocene climate of the northern margin of Saharan–Arabian Desert recorded in speleothems from the Negev Desert, Israel, Earth and Planetary Science Letters, 368, 88-100, http://dx.doi.org/10.1016/j.epsl.2013.02.027, 2013.

van Elteren, J. T., Šelih, V. S., Šala, M., Van Malderen, S. J., and Vanhaecke, F.: Imaging artifacts in continuous scanning 2D LA-ICPMS imaging due to nonsynchronization issues, Analytical chemistry, 90, 2896-2901, 2018.

van Elteren, J. T., Šelih, V. S., and Šala, M.: Insights into the selection of 2D LA-ICP-MS (multi) elemental mapping conditions, Journal of Analytical Atomic Spectrometry, 34, 1919-1931, 2019.

van Malderen, S.: Optimization of methods based on laser ablation-ICP-mass spectrometry (LA-ICP-MS) for 2-D and 3-D elemental mapping, Ghent University, 2017.

552 Vermeesch, P.: IsoplotR: A free and open toolbox for geochronology, Geoscience Frontiers, 2018.

553 von Quadt, A., Wotzlaw, J.-F., Buret, Y., Large, S. J., Peytcheva, I., and Trinquier, A.: High-precision
554 zircon U/Pb geochronology by ID-TIMS using new 10 13 ohm resistors, Journal of Analytical Atomic
555 Spectrometry, 31, 658-665, 2016.

556 Woodhead, J., and Petrus, J. J. G.: Exploring the advantages and limitations of in situ U–Pb carbonate
557 geochronology using speleothems, 1, 69-84, 2019.

558 Woodhead, J. D., and Hergt, J. M.: Strontium, neodymium and lead isotope analyses of NIST glass
559 certified reference materials: SRM 610, 612, 614, Geostandards Newsletter, 25, 261-266, 2001.

560 Wotzlaw, J.-F., Buret, Y., Large, S. J., Szymanowski, D., and von Quadt, A.: ID-TIMS U–Pb
561 geochronology at the 0.1‰ level using 10 13 Ω resistors and simultaneous U and 18 O/16 O isotope
562 ratio determination for accurate UO 2 interference correction, Journal of Analytical Atomic
563 Spectrometry, 32, 579-586, 2017.

564